BIOCHEMISTRY
including biophysical chemistry & molecular biology

Article

pubs.acs.org/biochemistry

An Iron–Sulfur Cluster Loop Motif in the *Archaeoglobus fulgidus* Uracil–DNA Glycosylase Mediates Efficient Uracil Recognition and Removal

Lisa M. Engstrom,[†] Olga A. Partington,[‡] and Sheila S. David*[,†]

[†]Department of Chemistry, University of California, Davis, One Shields Avenue, Davis, California 95616, United States

[‡]Department of Chemistry, University of Utah, Salt Lake City, Utah 84112, United States

Supporting Information

ABSTRACT: The family 4 uracil–DNA glycosylase from the hyperthermophilic organism *Archaeoglobus fulgidus* (AFUDG) is responsible for the removal of uracil in DNA as the first step in the base excision repair (BER) pathway. AFUDG contains a large solvent-exposed peptide region containing an α helix and loop anchored on each end via ligation of two cysteine thiolates to a $[4Fe–4S]^{2+}$ cluster. We propose that this region plays a similar role in DNA damage recognition as a smaller iron–sulfur cluster loop (FCL) motif in the structurally unrelated BER glycosylases MutY and Endonuclease III and therefore refer to this region as the "pseudo-FCL" in AFUDG. In order to evaluate the importance of this region, three positively charged residues (Arg 86, Arg 91, Lys 100) and the anchoring Cys residues (Cys 85, Cys 101) within this motif were replaced with alanine, and the effects of these replacements on uracil excision in single- and double-stranded DNA were evaluated. These results show that this region participates and allows for efficient recognition and excision of uracil within DNA. Notably, R86A AFUDG exhibited reduced activity for uracil removal only within double-stranded DNA, suggesting an importance in duplex disruption and extrusion of the base as part of the excision process. In addition, mutation of the $[4Fe–4S]^{2+}$ cluster cysteine ligands at the ends of the pseudo-FCL to alanine reduced the uracil excision efficiency, suggesting the importance of anchoring the loop via coordination to the cluster. In contrast, K100A AFUDG exhibited enhanced uracil excision activity, providing evidence for the importance of the loop conformation and flexibility. Taken together, the results herein provide evidence that the pseudo-FCL motif is involved in DNA binding and catalysis, particularly in duplex DNA contexts. This work underscores the requirement of an ensemble of interactions, both distant and in proximity to the damaged site, for accurate and efficient uracil excision.

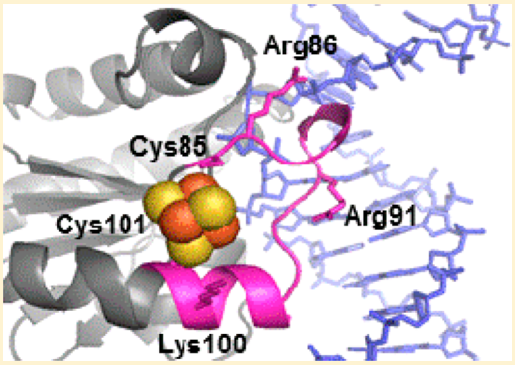

DNA repair pathways mitigate the detrimental effects of DNA modifications that occur through reactions with various endogenous and exogenous damaging agents.[1] Loss of the exocyclic amino group of cytosine by hydrolysis is one of the most common forms of DNA damage and is the primary mechanism of uracil accumulation in DNA.[2,3] Without repair, replication of the resulting G:U mismatch mediates formation of a permanent G:C to A:T transition mutation.[2] Nature, however, has evolved enzymes as part of the base excision repair (BER) pathway to prevent uracil-mediated mutations. The first repair step is initiated by a uracil DNA glycosylase (UDG), which recognizes and extrudes the uracil base into a specific extrahelical active site pocket, and then hydrolyzes the *N*-glycosidic bond to release free uracil. The resulting DNA abasic site is acted on by several other enzymes in the BER pathway to restore the original undamaged base pair.[1]

The UDGs belong to a superfamily of glycosylases, comprised of six distinct families.[4,5] The family 1 enzymes, particularly human (hUDG) and *E. coli* UDG (EcUDG), have been extensively studied[6−10] relative to family 4 and 5 UDGs. The family 4 and 5 UDGs are found almost exclusively in thermophilic and hyperthermophilic bacteria and archaea. This is significant in part because the rate of cytosine deamination is increased at higher temperatures.[11] However, the spontaneous mutation rate in thermophilic bacteria is similar to that of *E. coli*, suggesting an efficient uracil repair system. The first family 4 UDG was discovered in *Thermatoga maritima* (TMUDG), where the gene was found based on weak homology to family 2 UDGs.[12] Interestingly, most organisms that contain a family 4 UDG do not appear to contain any other type of UDG. Shortly after the discovery of TMUDG, several other thermophilic UDGs were identified and characterized including a family 4 UDG in the hyperthermophilic archaea *Archaeoglobus fulgidus* (AFUDG) as well as both a family 4 and 5 UDG in *Thermus thermophilus* (TTA and TTB, respectively).[13,14] The different UDG families have significant structural and sequence homology, particularly within the active site motifs. However,

Received: January 11, 2012
Revised: May 30, 2012
Published: May 31, 2012

dx.doi.org/10.1021/bi3000462 | *Biochemistry* 2012, 51, 5187–5197

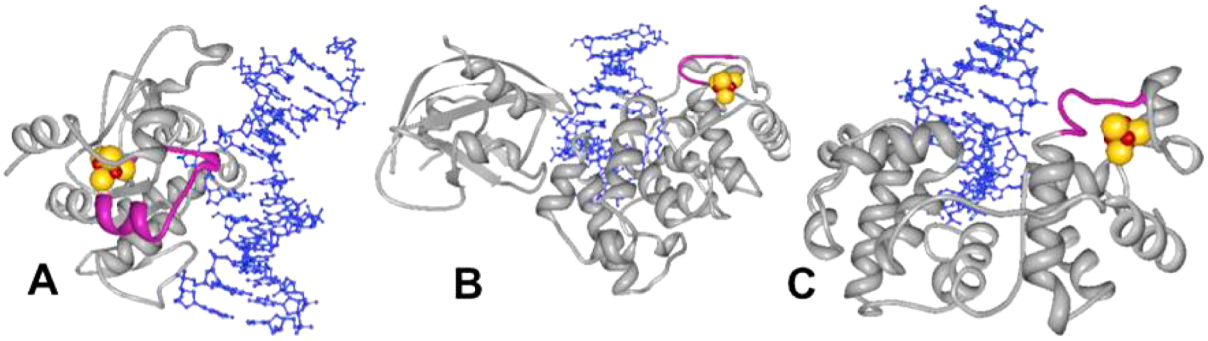

Figure 1. A view of the pseudo-FCL motif in TTB bound to abasic site DNA duplex (A) and the FCL motif in *B. stearothermophilus* MutY (B) and *E. coli* EndoIII bound to a substrate DNA (C). From structure coordinates deposited in the Protein Database, accession codes 2DDG, 1RRS, and 1ORP. Residues that make up the pseudo-FCL and FCL motifs are highlighted in fuschia, with bound DNA in blue. The $[4Fe-4S]^{2+}$ cluster is shown in spheres, yellow (S) and red (Fe).

the family 5 UDGs lack a polar residue in the active site at the position of the family 4 UDGs and are unable to cleave uracil from single-stranded DNA.

Despite having significant homology to the other UDG families, family 4 and 5 enzymes are the only members of the UDG superfamily that contain a $[4Fe-4S]^{2+}$ cluster.[15−18] However, a subset of enzymes within the helix−hairpin−helix (HhH) superfamily of BER glycosylases contain a $[4Fe-4S]^{2+}$ cluster cofactor.[19,20] Structural studies of two enzymes in this group, *E. coli* endonuclease (Endo) III and *E. coli* MutY, identified a solvent-exposed peptide loop (referred to as the iron−sulfur cluster loop, or FCL) formed by coordination of two cysteine thiolates to the $[4Fe-4S]^{2+}$ cluster.[21,22] The loop contains several positively charged residues that are in position to interact with the DNA phosphate backbone. Replacement of the positively charged residues in both enzymes established the participation of the FCL motif in efficient damage recognition and base removal. In Endo III, replacement of Lys 191 with Glu resulted in a >100-fold increase in K_m with no significant change in k_{cat}. Similarly, single substitutions of Arg 194, Lys 196, and Lys 198 with Ala in *E. coli* MutY resulted in decreased affinity for duplex DNA containing 8-oxo-7,8-dihydroguanosine (OG) or G paired with a noncleavable substrate analogue, 2′-deoxy-2′-fluoroadenosine. Notably, in the case of K198A MutY the rate of adenine removal opposite G measured under single-turnover conditions was also decreased indicating Lys 198 interactions with the DNA substrate contribute to efficient adenine excision.

Despite being structurally distinct from the HhH glycosylase superfamily, the family 4 and 5 UDGs contain a large peptide loop, which we propose plays a similar role as the FCL of MutY and Endo III (Figure 1). This loop, which we refer to henceforth as the "pseudo-FCL", is tethered on each end by coordination of two Cys ligands to the iron−sulfur cluster and contains three positively charged residues.[23] In order to investigate the role of the pseudo-FCL motif in AFUDG, the positively charged residues (Arg 86, Arg 91, Lys 100) and the two anchoring Cys ligands (Cys 85 and Cys 101) were replaced with alanine, and the consequences of these changes on the kinetics of uracil excision were evaluated (Figure 2). Our results demonstrate that mutations of residues within the pseudo-FCL alter substrate recognition and catalysis in a manner remarkably similar to analogous alterations in the FCL of the HhH glycosylases. This work underscores the intricate and complex nature of damage recognition, extrusion, and excision that require a complex array of interactions both distant and proximal to the active site.

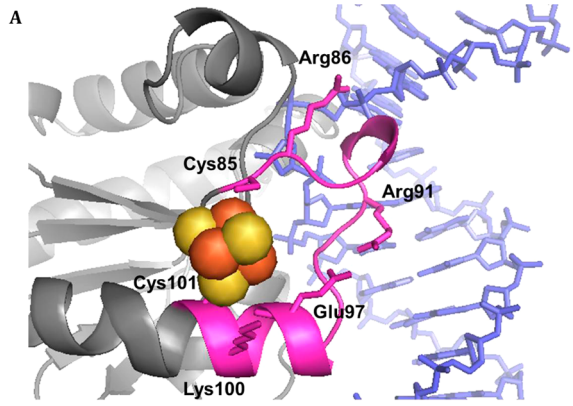

B

```
AFUDG     77 VYITNVLKCRPPNNRDPTPEEVEKCG-DYLVRQLEAIRP 114
PaUDGA    76 VFITNVVKCRPPNNRTPNREEVEACL-PYLIQQIGILKP 113
TTA       76 VYITNIVKCRPPQNRAPLPDEAKICTDKWLLKQIELIAP 114
TmUDG     81 VYICNVVKCRPPNNRTPTPEEQAACG-HFLLAQIEIINP 118
TTB      107 VYLTAAVRCAPPKNK-PTPEELRACA-RWTEVELGLLPE 143
PaUDGB   117 VYITSAVKCAPPKNR-PTAEEVYNCS-SWLREELEAVRP 153
```

Figure 2. Pseudo-FCL motif in family 4 and 5 UDGs. (A) Illustration of the close proximity of the pseudo-FCL motif (magenta) with duplex DNA (blue). The figure was generated by overlay of the structure coordinates of TTA (1UI0) and TTB cocrystallized with DNA (2DDG). Residue side chains that differed (Ile→Lys) were changed and numbered to correspond to those in AFUDG (see part B for alignment). The positively charged residues in AFUDG that were replaced by alanine are shown on the TTA structure in ball and stick representation. The [4Fe−4S] cluster is shown as spheres (Fe in orange, S in yellow). Note that only the side chains of the two Cys ligands that are part of the pseudo-FCL are shown. In addition, Cys 101 is coordinated to the iron that is behind the other three iron atoms and therefore is not visible. (B) Sequence alignments of the pseudo-FCL motif of various family 4 and 5 UDGs. Conserved cysteine residues that ligate the $[4Fe-4S]^{2+}$ cluster are highlighted in red, with positively charged residues within the pseudo-FCL motif highlighted in black.

EXPERIMENTAL PROCEDURES

Reagents and Chemicals. All chemicals were purchased from VWR or Fisher Scientific. [γ-^{32}P]-ATP was purchased from Perkin-Elmer and T4 polynucleotide kinase was purchased from New England Biolabs.

dx.doi.org/10.1021/bi3000462 | *Biochemistry* 2012, 51, 5187−5197

Enzyme Overexpression and Purification. The growth and purification were modified from a previously reported procedure.[15] AFUDG and TTB were overexpressed using the pET28a-*afung* plasmid containing the *afudg* gene[14] and the pET21d-*ttb* plasmid containing the *ttb* gene,[13] respectively, in BW(310)DE3 *E. coli* cells. Cells were grown in 4 L of LB growth media containing 34 μg/mL kanamycin at 37 °C until an OD_{600} of 0.6 was obtained. Protein expression was induced by the addition of 1 mM IPTG to the cell cultures, followed by incubation for 6 h at 30 °C. The cells were harvested by centrifugation (8000 rpm, 10 min, 4 °C) and the cell pellet resuspended in 40 mL of ice-cold 1X lysis buffer (25 mM Tris-HCl, 250 mM NaCl, pH 7.6) supplemented with 1 mM PMSF. The resuspended cell pellet was stored at −80 °C. For protein purification, cells were lysed by sonication and cellular debris removed by centrifugation (8000 rpm, 10 min, 4 °C). The supernatant was mixed with nickel−nitrilotriacetic acid (Ni-NTA) resin slurry (Qiagen, 3 mL/40 mL supernatant) by gentle rocking for 1 h at 4 °C. The protein-bound resin was then poured into two empty PD-10 columns (GE Healthcare) and washed with 25 mL of 2X lysis buffer, followed by 5 mL of 1X lysis buffer. Protein was eluted by addition of 2−5 mL of 1X lysis buffer containing 250 mM imidazole and the isolated eluate was then diluted 10-fold with buffer A (25 mM sodium phosphate buffer, 1 mM EDTA, pH 7). Subsequent purification steps were performed using an ÅKTA FPLC system. Using cation exchange chromatography (Hi Trap HPSP, GE Healthcare), the protein was eluted using a NaCl gradient by increasing the amount of buffer B (20 mM sodium phosphate buffer, 1 M NaCl, 1 mM EDTA, pH 7) from 0 to 100% over 6 column volumes. An additional purification step using a heparin affinity column was performed for TTB. For both AFUDG and TTB, eluted fractions were combined, buffer exchanged (20 mM sodium phosphate buffer, 100 mM NaCl, 1 M EDTA, 5% glycerol, pH 7.6) and concentrated using an Amicon Ultra-filtration Concentrator with 10 000 MWCO. The protein was diluted with glycerol (30% final concentration) and stored at −80 °C. Fractions were run on an SDS-PAGE to ascertain purity and found to be greater than 95% pure. The concentration of total protein was determined using ε_{280} = 28 318 M^{-1} cm^{-1} for AFUDG and ε_{280} = 28 900 M^{-1} cm^{-1} for TTB, and the concentration of the iron−sulfur cluster was determined for both enzymes using ε_{390} = 19 784 M^{-1} cm^{-1}.

AFUDG mutants were created using site-directed mutagenesis (Stratagene) to mutate each position individually to alanine. Correct incorporation of the mutation was confirmed by DNA sequencing. The mutants were then overexpressed and purified using the same procedures as wild-type AFUDG.

DNA Substrates. DNA containing standard nucleotides, 1′,2′-dideoxyribose (dSpacer or THF), and a C6 amino linker at the 5′-end were purchased from Integrated DNA Technologies. All oligonucleotides were either gel purified[24] or HPLC purified on a Beckman Gold Nouveau system using ion-exchange chromatography with a Waters AP1 DEAE 8HR column. The following oligonucleotide duplex was used in uracil excision assays: 5′-CGATCATGGAGCCACUAGCTCCCGTTACAG-3′·5′-CTGTAACGGGAGCTGGTGGCTCCATGATCG-3′. The following oligonucleotide sequences were used in fluorescence anisotropy assays: 5′-ACCGTGTGATAAA**X**-AAGGCGTTAAA-3′·5′-**Y**TTTAACGCCTTGTTTATCA-CACGGT-3′, where **X** = THF (tetrahydrofuran, an abasic site analogue) and **Y** = a C6 amino linker at the 5′-end that was covalently modified by X-rhodamine-5,6-isothiocyanate (Invitrogen).[25]

AFUDG Active Fraction Assays. The amine-modified oligonucleotide (100 μg) was purified by chloroform extraction followed by ethanol precipitation. The precipitate was dried briefly under vacuum and then resuspended in 12 μL of H_2O. The rhodamine-5,6-isothiocyanate (250 μg) was dissolved in 14 μL of DMF and added to the amino-modified oligonucleotide in addition to 75 μL of freshly prepared sodium bicarbonate buffer, pH 9. The resulting mix was allowed to shake at room temperature overnight. The labeled oligonucleotide was ethanol precipitated, and the resulting pellet dried briefly by rotary evaporation. The labeled oligonucleotide was purified by gel electrophoresis on a 20% denaturing polyacrylamide gel.[24] The THF-containing strand was then annealed to its complement containing the rhodamine label, creating a THF:G central base pair, by combining both strands in annealing buffer (125 mM Tris-HCl, 125 mM NaCl, 5 mM EDTA, pH 7.6), heating at 90 °C for 10 min, and allowing to cool slowly to room temperature overnight.

Anisotropy measurements were obtained using a PTI fluorescence anisotropy instrument equipped with a 75 W xenon arc lamp, an excitation monochromator, and dual emission monochromators. The excitation wavelength was set to 580 nm with a band-pass of 4 nm leading to the PMT. Both emission detectors were set to a wavelength of 610 nm with a band-pass of 2 nm leading to the PMT. The cuvette chamber was set to a constant 25 °C using a temperature controller unit (Quantum Northwest). Rhodamine-labeled substrate (500 nM) in 1X UDG buffer (25 mM Tris-HCl, 1 mM EDTA, pH 7.6) was added to the cuvette to calculate the *g*-factor. Anisotropy values were calculated as previously reported.[25,26] WT AFUDG was titrated into the DNA reaction mix in increasing concentrations, and after 1 min incubation, anisotropy measurements were recorded every second over a period of 30 s for each addition of enzyme. These results were then averaged to give the anisotropy for that particular enzyme concentration. The enzyme concentration was corrected for the dilution factor and plotted against anisotropy values using Microsoft Excel. The active enzyme concentration was calculated as a percentage of the total protein concentration (determined by UV−vis spectroscopy using ε_{280} = 28 318 M^{-1} cm^{-1}).

Uracil Glycosylase Assays. The 5′-end of the uracil containing strand was labeled with [γ-^{32}P]-ATP using T4 polynucleotide kinase (New England Biolabs). Excess ATP was removed using a MicroSpin G-50 spin column (GE Healthcare). The uracil containing oligonucleotide was then annealed to its complement by adding 20% excess complement and heating at 90 °C for 10 min followed by slow cooling overnight in annealing buffer (125 mM Tris, pH 7.5, 125 mM NaCl, 5 mM EDTA). Radiolabeled U-containing duplex DNA was mixed with non-radiolabeled U-containing DNA to afford a stock solution of 0.5−5% labeled uracil-containing DNA. This was used to make the appropriate concentration of DNA for the various experiments. Aliquots were removed at designated times and quenched in NaOH followed by heating at 90 °C for 10 min. An equal volume of formamide loading dye (80% formamide, 0.025% xylene cyanol, 0.025% bromophenol blue in Tris-Borate-EDTA [TBE] buffer) was added to each aliquot and incubated for an additional 10 min at 90 °C. The samples were run on a 15% denaturing polyacrylamide gel in 1X TBE at 1500 V for 2 h to separate the 14-nucleotide strand (derived

dx.doi.org/10.1021/bi3000462 | *Biochemistry* 2012, 51, 5187−5197

from the product) from the 30-nucleotide strand (derived from the substrate). The gels were exposed to phosphor storage screens overnight and scanned on a Typhoon Trio imager. Bands were quantified using ImageQuaNT (v.5.2), and data were fit using GraFit (v.5).

Single-turnover reactions were carried out using a KinTek Rapid Quench instrument. Reactions were incubated at 52 °C using a circulating water bath with a digital controller. Uracil-containing duplex (20 nM) in 1X UDG buffer (25 mM Tris-HCl, 1 mM EDTA, pH 7.6) was rapidly mixed with equal amounts of sample containing 400 nM active AFUDG, 12.5 nM nonspecific DNA, in 1X UDG buffer. The final concentration of NaCl is 30 mM from the DNA duplex solution. Aliquots were removed from the reaction at designated times and quenched by the addition of 0.5 M NaOH, followed by heating at 90 °C for 10 min. An equal volume of formamide loading dye was added, and the aliquots were incubated an additional 10 min at 90 °C. Samples were electrophoresed and quantified as described above. The resulting plots of product formed as a function of time were fitted to a single-exponential equation using GraFit. To ensure that the reaction conditions were appropriate for determination of k_2, several enzyme concentrations were tested to ensure that the conditions provided the maximal observed rate.

Steady-state uracil glycosylase assays were performed using 1 nM active AFUDG (activity determined by fluorescence anisotropy assays), while the concentration of DNA was varied from 10 to 200 nM uracil-containing DNA duplex. Reactions were performed in UDG Buffer by incubating the DNA-containing reaction mix at 52 °C and mixing with the appropriate amount of enzyme. Aliquots were removed at designated time points and quenched by addition of NaOH to give a final concentration of 0.2 M, followed by heating at 90 °C for 10 min. PAGE analysis and quantitation of gels was as described above. Complete time courses were used and the data fit to a single-exponential equation. Velocity as a function of substrate concentration was fitted using the Michaelis–Menten equation.[27]

For both multiple-turnover and active-site titration assays with TTB, 20 nM duplex DNA was equilibrated at 52 °C in 1X UDG buffer (25 mM Tris-HCl, 25 mM NaCl, 1 mM EDTA) and an appropriate amount of TTB, ranging from 2 to 10 nM, was added to afford 10–20% product formation for the burst phase of the reaction. Reactions were fit with the appropriate rate equations analogous to that reported previously by our laboratory for MutY.[28]

Electron Paramagnetic Resonance Spectroscopy of C85A, C101A, and WT AFUDG. Samples were prepared by incubating enzyme (60–100 μM cluster-containing enzyme, determined by UV–vis spectroscopy using ε_{390} = 19 784 M^{-1} cm^{-1}) for 10 min at 52 °C. The samples were immediately loaded into an EPR sample tube and frozen in liquid nitrogen. All samples were prepared in 20 mM sodium phosphate buffer, pH 7.6, 30 mM NaCl, 1 mM EDTA, 15% glycerol. Samples were run on a Bruker ESP-300 X-band EPR spectrometer with an Oxford Instruments ESR-900 helium-flow cryostat. Parameters were as follows: microwave frequency, 9.696 GHz; microwave power, 5.09 mW; modulation amplitude, 7.94 mT; sample temperature, 10 K; receiver gain, 2.0×10^4; with 5 scans performed for each spectrum. Samples were integrated using the double integration method with IgorPro, using 100 μM CuEDTA as a standard.

RESULTS

General Features of Uracil Removal Activity of AFUDG and TTB. Although the family 4 and 5 UDGs share a significant amount of homology in both sequence and structure, they display distinctly different features in terms of the processing of uracil-containing substrates. The glycosylase activity of the family 4 AFUDG and the family 5 TTB was examined using a 30 nt uracil-containing oligonucleotide labeled on the 5′-end using [γ-^{32}P]-ATP and annealed to the appropriate complement to create a U:G bp-containing substrate. Under multiple turnover (MTO) conditions ([E] < [DNA]) with the U:G duplex substrate, the reaction with TTB exhibits biphasic kinetics, distinguished by the observation of a rapid exponential burst of product, followed by a slower linear formation of product (Figure 3). This type of biphasic behavior

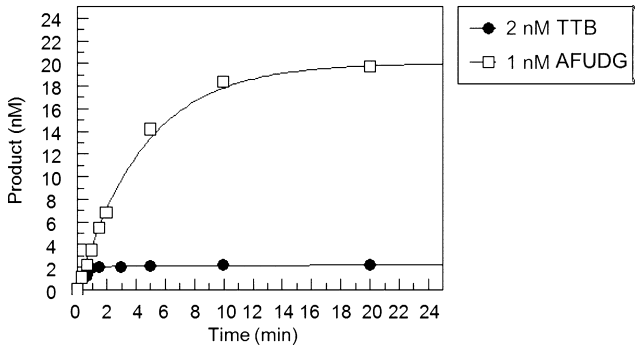

Figure 3. Uracil excision from duplex substrates with TTB and AFUDG under multiple-turnover conditions. AFUDG exhibits fast substrate turnover resulting in depletion of substrate within the time frame measured, while under similar conditions TTB displays biphasic kinetic behavior due to slow DNA product release. AFUDG (1 nM) and TTB (2 nM) incubated with 20 nM uracil-containing duplex DNA, incubated at 52 °C in 20 mM Tris-HCl, 30 mM NaCl, 1 mM EDTA.

is similar to that seen with several DNA glycosylases and is likely due to slow release of the DNA product by TTB.[13,17,28] On the basis of the similarity to the catalytic behavior of the MutY glycosylase,[28] we utilized an analogous approach and minimal kinetic scheme (Scheme 1) depicting three basic steps

Scheme 1

$$\mathrm{UDG + (DNA)_s} \underset{k_{-1}}{\overset{k_1}{\rightleftharpoons}} \mathrm{UDG{\bullet}(DNA)_s} \xrightarrow{k_2} \mathrm{UDG{\bullet}(DNA)_p} \xrightarrow{k_3} \mathrm{UDG + (DNA)_p}$$

in the enzymatic cycle: substrate binding (k_1 and k_{-1}), chemical step(s) involved in cleavage of the *N*-glycosidic bond (k_2), and product release (k_3). Under MTO conditions where substrate DNA (20 nM) is in excess over the concentration of TTB (2 nM active enzyme), the rate of product release, k_3, was determined to be 0.004 ± 0.002 s^{-1}. Of note, consistent with previous observations, we found that TTB was not able to remove uracil from single-stranded DNA.[13,17] In contrast, under these same conditions AFUDG shows full conversion of all substrate to product (Figure 3). This indicates that the rate of product release is sufficiently fast to allow for multiple enzyme turnovers leading to substrate depletion. Furthermore, the activity was amenable to analysis at a variety of substrate concentrations to allow for determination of Michaelis–Menten steady-state parameters k_{cat} and K_m (*vide infra*).

dx.doi.org/10.1021/bi3000462 | *Biochemistry* 2012, 51, 5187–5197

These differences in kinetic activity provided an opportunity to use several approaches to analyze and determine quantitative information about the kinetic behavior of AFUDG and TTB.

Active Fraction Assay. The ability to determine the active fraction of an enzyme is important when comparing kinetic rate constants, as the amount of product formation observed is dependent on the concentration of active enzyme rather than the amount of total protein present in a sample. Because of the observation of a defined burst phase with TTB under MTO conditions that increases proportionately with the amount of enzyme added, the concentration of active protein can be determined from the amplitude of this burst phase.[29] As shown in Figure 3, AFUDG does not exhibit a defined burst under MTO conditions and therefore requires an alternative approach to determine the concentration of active enzyme.

To this end, a fluorescence anisotropy-based method was developed to approximate the active enzyme fraction by determining the amount of purified WT AFUDG that is competent to bind a DNA duplex containing a centrally located abasic site product analogue (THF) base-paired across from G. The duplex was labeled with X-rhodamine (RhX) on the 5′-end of the strand complementary to the strand containing the THF nucleotide. The change in fluorescence anisotropy of RhX (500 nM duplex) was monitored as a function of added enzyme (200−5000 nM) and was found to increase linearly and then plateau (Figure 4). Similar titrations performed at several lower DNA concentrations indicated that these conditions were above the dissociation constant of AFUDG with the THF-containing duplex (K_d < 20 nM) and therefore provide conditions where percent bound correlates with "active" AFUDG concentration.[29] Based on the break-point from a minimum of three separate titrations, the fraction competent to bind DNA was calculated for each enzyme preparation (Figure 4). This active fraction from several separate preparations of WT AFUDG was fairly high, varying between 65% and 80% active. This active enzyme concentration was used in all subsequent glycosylase activity assays.

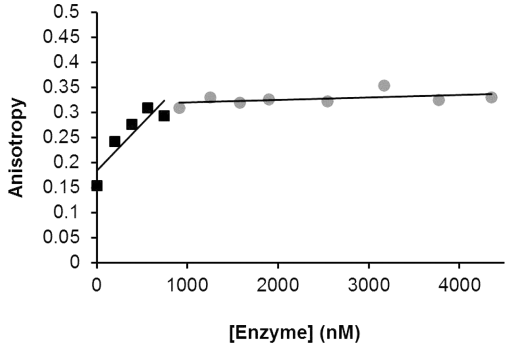

Figure 4. Representative graph of binding titrations of AFUDG with RhX-product analogue ds DNA using fluorescence anisotropy. Reaction conditions as follows: [DNA] = 500 nM, [NaCl] = 30 mM, reactions incubated at 25 °C. Active fraction was determined from an average of at least three independent titrations.

In order to validate the use of fluorescence anisotropy binding assays in approximating the active site concentration of AFUDG, similar experiments were performed using TTB and compared to the active site fraction determined by analysis of the burst amplitudes from MTO experiments. The active fraction determined using the burst amplitudes from MTO uracil excision assays with TTB at 37 °C (40 ± 6%) was within error of the active fraction determined by fluorescence anisotropy (42 ± 1%) at 25 °C (Figure 5). The similar results are notable since uracil excision burst amplitudes report on the amount of substrate that can be catalytically processed by the enzyme, while fluorescence anisotropy experiments determine the amount of enzyme that is competent to bind the product analogue duplex. Not only does this support the use of binding to the product analogue via fluorescence anisotropy for gauging the active site concentration, it also suggests that the inactive enzyme is incapable of binding to the DNA duplex.

Overexpression, Active Site Titration, and Stability of R86A, R91A, K100A, C85A, and C101A AFUDG. In order to test whether the pseudo-FCL motif in AFUDG participates in a manner analogous to that of the FCL in MutY and Endo III, site-directed mutagenesis was used to individually replace the positively charged residues and the anchoring Cys ligands with alanine. The resulting mutated AFUDG enzymes were overexpressed in *E. coli* and purified in a manner similar to the WT protein. While K100A AFUDG expressed at levels similar to WT, the other mutants (R86A, C101A, C85A) generally had lower levels of overexpression and yield after purification (~20% of WT). The ability to overexpress the two Cys-to-Ala mutants was somewhat surprising since these forms lack a ligand that can coordinate the $[4Fe-4S]^{2+}$ cluster, and previous work in our laboratory had shown that analogous mutated *E. coli* MutY enzymes were not readily overexpressed.[30] Similar to

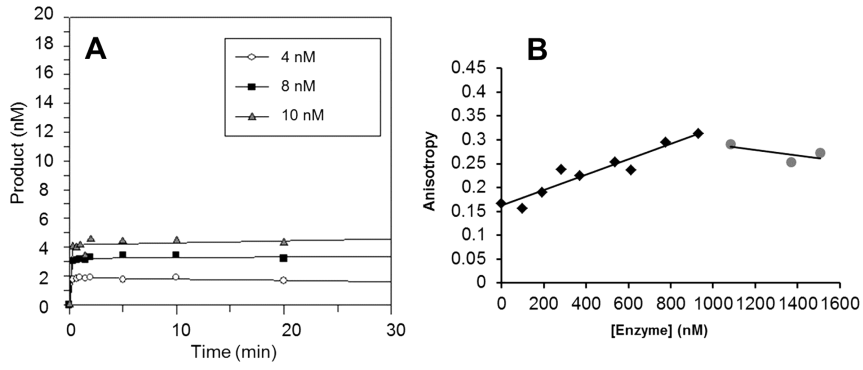

Figure 5. Active fraction of TTB determined from glycosylase activity and fluorescence anisotropy binding titrations. (A) Active fraction determined from burst amplitudes for MTO reactions under the following conditions: TTB (2 nM, 4 nM, 8 nM) incubated with 20 nM uracil-containing duplex DNA, incubated at 37 °C. (B) Anisotropy reactions were carried out as follows: [DNA] = 500 nM, [NaCl] = 30 mM, reactions incubated at 25 °C. Active fraction determined from an average of at least three independent titrations.

dx.doi.org/10.1021/bi3000462 | *Biochemistry* 2012, 51, 5187−5197

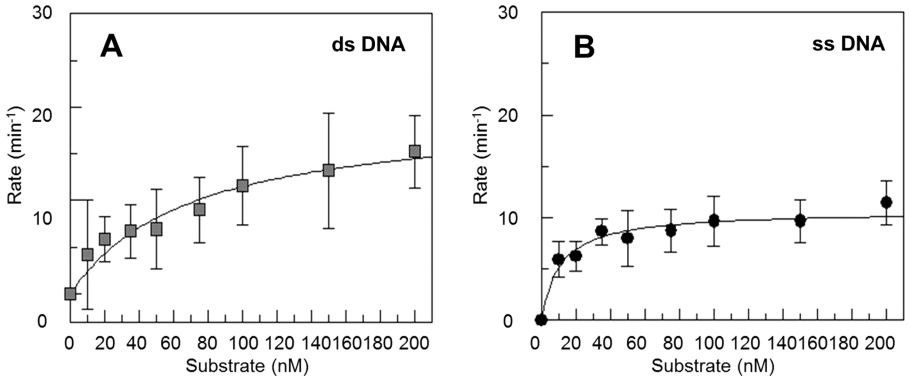

Figure 6. Multiple-turnover glycosylase activity of AFUDG. (A) Representative data for AFUDG-catalyzed uracil excision from a double-stranded DNA containing a centrally located U:G mispair. (B) Representative data for AFUDG catalyzed uracil excision from a single-stranded DNA containing a centrally located uracil. For both single- and double-stranded experiments, reaction conditions were as follows: [E] = 1 nM, [DNA] = 10−200 nM, reactions incubated at 52 °C. The lines indicate the best fit to the Michaelis−Menten equation, and relevant k_{cat} and K_m parameters from at least three separate experiments are listed in Table 1.

the WT enzyme, both C101A and C85A retained the absorption band centered at 390 nm due to cysteinate-to-Fe(III) charge transfer transitions of the $[4Fe{-}4S]^{2+}$cluster cofactor. EPR analysis of both mutants showed the presence of some $[3Fe{-}4S]^{1+}$ cluster, indicating lability of the uncoordinated iron (Supporting Information, Figure S1). In the case of R91A AFUDG, a very small amount of colorless protein was isolated after purification. The absence of the distinctive yellow color of the protein sample indicated loss of the iron−sulfur cluster, and therefore, this mutated enzyme was not analyzed further.

The K100A mutant was able to bind the THF-containing DNA, although the amount of active protein (~14%) was lower than commonly seen with the WT enzyme. The fluorescence anisotropy data indicated that both C85A and C101A mutants are able to bind DNA; however, the plateau region was not as well-defined as those observed with the WT and K100A enzyme. This provided an estimated percent active fraction relative to total protein of approximately 25 and 9 for C85A and C101A, respectively. In contrast, the titration curve failed to reach saturation even at extremely high protein concentrations (7 μM protein) in the anisotropy binding assays with R86A AFUDG. These results indicate a severe binding reduction caused by the Arg 86 to Ala mutation.

Because of the absence of a fully coordinated $[4Fe{-}4S]^{2+}$ cluster in C85A and C101A AFUDG, we anticipated that these mutated enzymes may be less stable than the WT enzyme. Thus, in order to determine the relative stability of C85A, C101A, and K100A relative to WT, the enzymes were incubated in assay buffer and aliquots removed at defined times. The observed rate of reaction was determined using 1 nM enzyme and 10 nM U:G-containing DNA. The observed rate for each enzyme was normalized to the rate observed without preincubation in assay buffer and evaluated over a time course of 10 min (Figure S2). Both C85A and C101A AFUDG were found to lose considerable activity after incubation in assay buffer for 2 min, with ~20% of the original level of activity remaining. In contrast, K100A retained ~80% of the activity of the WT enzyme during incubation for the same time frame.

Because of the inability to determine an accurate enzyme concentration for R86A and instability of C85A and C101A, steady-state experiments were not performed with these enzymes since determination of k_{cat} relies on accurate enzyme concentration and the steady-state reactions occur over a long time period (40 min). However, single-turnover rate constants are pseudo-first-order rate constants and therefore less dependent on the exact enzyme concentration. In addition, with AFUDG and the mutated forms examined herein, STO reactions are completed within a short time period (1 min).

Steady-State Kinetics of WT and K100A AFUDG. The steady-state kinetic parameters describing uracil excision by WT and K100A AFUDG were examined using a single-stranded 5′-[^{32}P]-phosphate-labeled oligonucleotide containing a central uracil, either alone or annealed to a complementary strand, creating a central U:G mispair. Using enzyme concentration corrected for active fraction, 1 nM active enzyme was used in all experiments, with the concentration of DNA (either single- or double-stranded) ranging from 10 to 200 nM. Velocities were determined as a function of substrate concentration and then plotted versus the corresponding substrate concentrations (Figure 6, Table 1). The data were fit using the Michaelis−Menten equation.[27] The rate of catalytic turnover, k_{cat}, was found to be higher with double-stranded (ds) substrate compared to single-stranded (ss) substrate (20 min^{-1} vs 11 min^{-1}, respectively). However, AFUDG has significantly different K_m values for the two substrates, with values of 70 ± 20 nM for ds DNA and 11 ± 3 nM for ss DNA. Consequently, AFUDG has higher catalytic efficiency (k_{cat}/K_m) toward ss DNA due to the smaller K_m value (Table 1).

Table 1. Kinetic Parameters for WT and K100A AFUDG Using a Single-Stranded U and Double-Stranded U:G Base Pair Substrate Determined under Steady-State and Single-Turnover Conditions[a]

	V_{max} (nM/min)	K_m (nM)	k_{cat} (min^{-1})	k_{cat}/K_m (nM^{-1} min^{-1})	k_2 (min^{-1})
WT, ds	20 ± 2	70 ± 20	20	0.29	40 ± 3
K100A, ds	51 ± 5	54 ± 13	51	0.94	55 ± 4
WT, ss	11 ± 1	11 ± 3	11	1	28 ± 2
K100A, ss	16 ± 1	8 ± 3	16	2	46 ± 1

[a]Reaction conditions: [E] = 1 nM (steady-state reactions), ≥400 nM (single-turnover reactions), [DNA] = 10−200 nM (steady state), 20 nM (single turnover), reactions incubated at 52 °C in 25 mM Tris-HCl, 30 mM NaCl, 1 mM EDTA, pH 7.6. The sequence of the uracil-containing oligonucleotide is listed in the methods.

dx.doi.org/10.1021/bi3000462 | Biochemistry 2012, 51, 5187−5197

The uracil excision activity of K100A was analyzed under steady-state conditions in a manner analogous to the WT enzyme. Surprisingly, the rate of catalytic turnover was increased with the K100A mutant compared to WT AFUDG, with k_{cat} values of 16 and 51 min^{-1} for ss and ds DNA substrates, respectively (Table 1). K100A and WT AFUDG exhibit similar affinities to each other for duplex (K_m = 54 ± 13 and 70 ± 20 nM, respectively) and single-stranded DNA (K_m = 8 ± 3 and 11 ± 3 nM, respectively). In fact, the mutation has not altered the ss to ds preference in terms of binding; both enzymes exhibit higher affinity for ss DNA (Table 1). However, k_{cat}/K_m is increased in K100A compared to WT due to the increased V_{max} values (Table 1). Overall, this results in a 3-fold and 2-fold increase in catalytic efficiency (k_{cat}/K_m) for K100A over WT for ds and ss substrates, respectively.

Single-Turnover Uracil Excision by AFUDG and Pseudo-FCL Mutants. Single-turnover (STO) reactions ([E] > [DNA]) were performed with WT AFUDG and the pseudo-FCL mutants in order to determine the rate constant k_2, which includes all steps up to and including base excision (Scheme 1). Importantly, these measurements remove any influence of product release that may be dominating k_{cat}. STO experiments with AFUDG were performed using double- and single-stranded DNA, and with TTB using double-stranded DNA (Figure 7, Table 2). In all cases, the reactions followed first-order kinetics, and the reaction progress curves were fitted to single exponentials.[28] Notably, several enzyme concentrations were examined to establish that the maximal k_{obs} had been achieved to permit k_{obs} to be equated with k_2. AFUDG was able to cleave uracil from duplex DNA faster than TTB, with k_2 values of 40 ± 3 and 28 ± 2 min^{-1}, respectively (Table 2). The rate of uracil cleavage from ss DNA by AFUDG was found to be 28 ± 2 min^{-1} (Table 2). Consistent with the observation of a defined burst with TTB acting on the ds DNA substrate, the rate of glycosidic bond cleavage (k_2) is significantly faster than the rate of product release (k_3 = 0.004 ± 0.002 min^{-1}). The fact that k_2 is greater than k_{cat} with both ss and ds DNA suggests that product release is also rate-limiting for AFUDG; however, the magnitude of the difference in k_2 versus k_3 must be small due to the only 2-fold difference in k_{cat} and k_2 and the lack of an observed burst phase under MTO conditions.

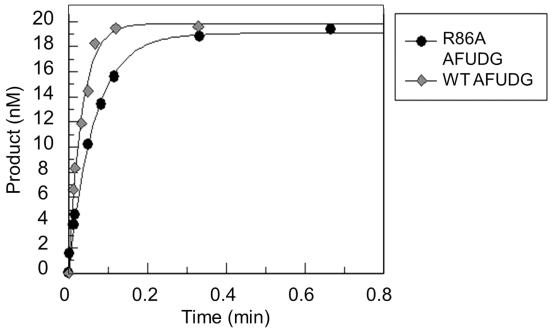

Figure 7. Representative plots of single-turnover excision of uracil in ds DNA by WT and R86A AFUDG. Lines represent fitting to a single exponential as described in the methods. At least three independent trials were used to determine values for k_2 listed in Tables 1 and 2. For both single- and double-stranded experiments, reaction conditions were as follows: [E] ≥ 400 nM, [DNA] = 20 nM, reactions incubated at 52 °C in 25 mM Tris-HCl, 30 mM NaCl, 1 mM EDTA, pH 7.6.

Table 2. Rate Constants of Uracil Excision Determined for AFUDG and Pseudo-FCL Mutants Using Single-Stranded U-Containing or Double-Stranded U:G Base Pair-Containing Substrates under Single-Turnover Conditions[a]

	ds, k_2 (min^{-1})	ss, k_2 (min^{-1})
TTB	28 ± 2	N.D.
AFUDG	40 ± 3	28 ± 2
R86A AFUDG	15 ± 1	27 ± 4
K100A AFUDG	55 ± 4	46 ± 1
C85A AFUDG	17 ± 1	10 ± 1
C010A AFUDG	24 ± 3	18 ± 1

[a]Reaction conditions: [E] ≥ 400 nM, [DNA] = 20 nM, reactions incubated at 52 °C in 25 mM Tris-HCl, 30 mM NaCl, 1 mM EDTA, pH 7.6.

Single-turnover reactions with K100A AFUDG were carried out in a manner analogous to reactions performed with WT AFUDG. These measurements show that K100A has an *increased* rate of glycosidic bond cleavage (k_2) for both double- and single-stranded substrates, with k_2 values of 55 ± 4 and 46 ± 1 min^{-1}, respectively (Table 2). Notably, with this mutant both k_2 and k_{cat} are increased, indicating that the measured rate under steady-state conditions is likely due to an increase in both the rate(s) for base excision step(s) and the rate of product release.

Despite the compromised ability to bind to the product duplex revealed via the anisotropy experiments, R86A AFUDG was found to be rather efficient at removing uracil from both ds and ss DNA under the conditions of the single-turnover glycosylase assays. Indeed, the reactions with R86A AFUDG proceeded at rates too fast to measure by manual assay, similar to WT AFUDG (Figure 7). However, these measurements revealed that the rate constants for uracil excision by R86A AFUDG (k_2 = 15 ± 1 min^{-1}) from the ds substrate are decreased 2.5-fold compared to those measured under the same conditions with the WT enzyme (Table 2). This suggests that the binding deficiency caused by the mutation may be compensated to a significant extent at high enzyme concentrations; however, the fact that the maximum observed rate (i.e., k_2) is still less than that observed for the WT enzyme suggests that this residue provides interactions with the DNA substrate that are important for facilitating uracil cleavage. Surprisingly, under STO conditions, R86A AFUDG was able to remove uracil from within single-stranded DNA with a similar efficiency as observed with WT AFUDG, with a rate constant k_2 of 27 ± 1 min^{-1}.

The replacement of the two cysteine ligands bracketing the end of the pseudo-FCL with alanine resulted in a decreased ability to remove uracil compared to WT under single-turnover conditions, both in a double- and single-stranded context. C85A AFUDG had ~2.5-fold lower rates of glycosidic bond cleavage, with k_2 of 17 ± 1 and 10 ± 1 min^{-1} for double- and single-stranded DNA, respectively (Table 2). Rates of glycosidic bond cleavage were decreased ~1.5-fold compared to WT for C101A, with k_2 values of 24 ± 3 min^{-1} for uracil in double-stranded DNA and 18 ± 1 min^{-1} for single-stranded DNA (Table 2). The observed reduction in activity due to the subtle absence of one of the $[4Fe-4S]^{2+}$ cluster Cys ligand anchors of the loop provides further support for participation of this pseudo-FCL motif of AFUDG in uracil excision.

dx.doi.org/10.1021/bi3000462 | *Biochemistry* 2012, 51, 5187−5197

DISCUSSION

Since the discovery of the first uracil DNA glycosylase in 1974,[31] extensive studies have defined detailed features of its uracil recognition and excision.[32,33] Though many of the features of the prototypical UDG are shared with UDG superfamily members,[4] an obvious difference of family 4 and 5 UDGs is the presence of an iron−sulfur cluster.[16] The $[4Fe-4S]^{2+}$ cluster in the HhH BER glycosylases MutY and Endo III, as well as AFUDG, is redox active in the presence of DNA, suggesting that DNA binding alters the environment around the cluster permitting cluster oxidation.[15] In addition, it has been shown that interactions of positively charged amino acids within the iron−sulfur cluster loop (FCL) motif of MutY and the negatively charged DNA backbone play an important role in both recognition and repair of damaged DNA.[21] We reasoned that an analogous but larger loop region in the family 4 and 5 UDGs may play a similar role in damage recognition and removal. Indeed, this work identifies this "pseudo-FCL" in AFUDG as a novel motif that participates in damage removal. Replacements of the positively charged residues (Arg 86, Arg 91, Lys 100) and the two Cys ligand anchors in the pseudo-FCL to alanine were shown to alter protein stability, DNA binding, and catalysis. These findings underscore the complexity associated with damaged DNA recognition and the intricate interactions required for proper repair.

As an important first step in this work, we evaluated the kinetics of WT AFUDG under steady-state and single-turnover conditions with both ds and ss uracil-containing oligonucleotides. Although there are slight differences between the two substrates, this work demonstrates the proficiency of AFUDG to remove uracil from both double- and single-stranded DNA contexts. Indeed, k_{cat} values indicate a 2-fold faster rate of processing of ds substrates, but K_m values were ∼6-fold reduced for the ss substrates. This provides a specificity constant (k_{cat}/K_m) that is 3-fold greater for the ss uracil-containing substrate. In addition, the rate constants (k_2) measured under single-turnover conditions showed similar magnitudes of efficient excision in both ds and ss contexts, with a slightly faster rate of excision in the former. Studies have shown that humans utilize different UDGs at distinct points in the cell cycle, some more closely linked to transcription while others are involved more widely in BER.[34,35] Given that AFUDG is the only UDG found in *A. fulgidus*, the ability of AFUDG to act efficiently on both double- and single-stranded DNA suggests a potential role during replication and/or transcription-associated repair. Proper repair prior to replication is critical since uracil does not block DNA replication and is miscoding.

Several groups have previously reported k_{cat} and K_m values for AFUDG, although the absolute values reported are quite different from those reported herein.[14,36] Notably, the relative processing of ss versus ds substrates based on our analysis and the previous studies are similar. The difficulties in comparing directly with these previous reports are due to several issues. One issue is that the previous analyses with AFUDG were performed at different temperatures and buffer conditions and under conditions that may not have been truly "steady state" (e.g., enzyme concentration was too high). Such differences may be further exacerbated by use of total rather than active enzyme concentrations. Indeed, our work presents a method to determine the active fraction of AFUDG utilizing fluorescence anisotropy. Using this method, kinetics of WT AFUDG from different preparations and different laboratories may be more readily compared.

The kinetic analysis of WT AFUDG provided a basis for examining specific mutated AFUDG enzymes to evaluate our hypothesis that the pseudo-FCL motif in AFUDG plays a role in damage recognition and repair. The low overexpression of R91A and absence of the Fe−S cluster suggests that Arg 91 is required for proper folding and insertion of the iron−sulfur cluster cofactor. The importance of Arg 91 is likely due to formation of a salt bridge with another conserved residue within the pseudo-FCL motif, Glu 97, observed in the homology modeled structure (Figure 2). The presence of ion pairs and salt bridges are often used in thermophilic enzymes to increase protein stability.[37] It is possible that in a cellular context the presence of DNA may alter this key salt-bridge interaction, allowing Arg 91 to interact with DNA. This idea is based on the cocrystal structure of TTB with duplex DNA, where a Lys residue at the position corresponding to Arg 91 is flipped toward the DNA backbone within hydrogen bonding distance, yet the conserved Glu remains in the same position as in the TTA structure. Thus, Arg 91 in AFUDG may be similarly positioned for DNA binding. Of note, Lys or Arg in this position is conserved among all family 4/5 UDGs, suggesting a critical function for a positively charged residue at this position (Figure 2B).

The unexpected *increased* catalytic efficiency (k_{cat}/K_m) of K100A over WT AFUDG provides support for participation of the pseudo-FCL in uracil excision. The complete processing of uracil-containing substrates by AFUDG requires a number of different steps, including DNA binding, nucleotide flipping, uracil cleavage, and product release, all of which would have distinct microscopic rate constants. However, the rate of catalysis (k_{cat}) will be dominated by the rate-determining step. For WT AFUDG, the rate of glycosidic bond cleavage (k_2) is greater than k_{cat}, indicating that product release is rate limiting. With the K100A mutant, k_2 and k_{cat} are within error of each other with the double-stranded DNA substrate, suggesting that product release is no longer rate limiting with this substrate. Although this increases the overall catalytic efficiency (k_{cat}/K_m) of K100A AFUDG, faster product release would not necessarily be beneficial, since improper release of the abasic product would result in the release of a highly cytotoxic product capable of producing more damage in the form of single-strand breaks.[2,28] Notably, K100A also exhibited significantly increased rates of glycosidic bond cleavage (k_2) with both ds and ss uracil substrates compared to the WT enzyme, suggesting that the Lys substitution influences the intrinsic uracil excision process. The enhanced activity resulting from replacement of the positively charged Lys with Ala makes it unlikely that the Lys side chain directly interacts with the substrate DNA. However, modifications at this position may enhance the ability of the pseudo-FCL motif to engage substrate DNA. Lys 100 is located adjacent to Cys101, one of the Cys residues that anchors the pseudo-FCL motif. Replacement of lysine with alanine would be expected to stabilize the alpha helical segment of the pseudo-FCL. The solvent-exposed pseudo-FCL is likely a dynamic region of AFUDG and therefore sensitive to changes that alter conformational flexibility. Consistent with the indirect effect of the Lys-to-Ala mutation in AFUDG, at this position in family 4/5 UDGs an Ala residue is more commonly found than Lys (Figure 2B).

Consistent with the importance of Arg 86, this residue is strictly conserved among family 4 UDGs (Figure 2B).

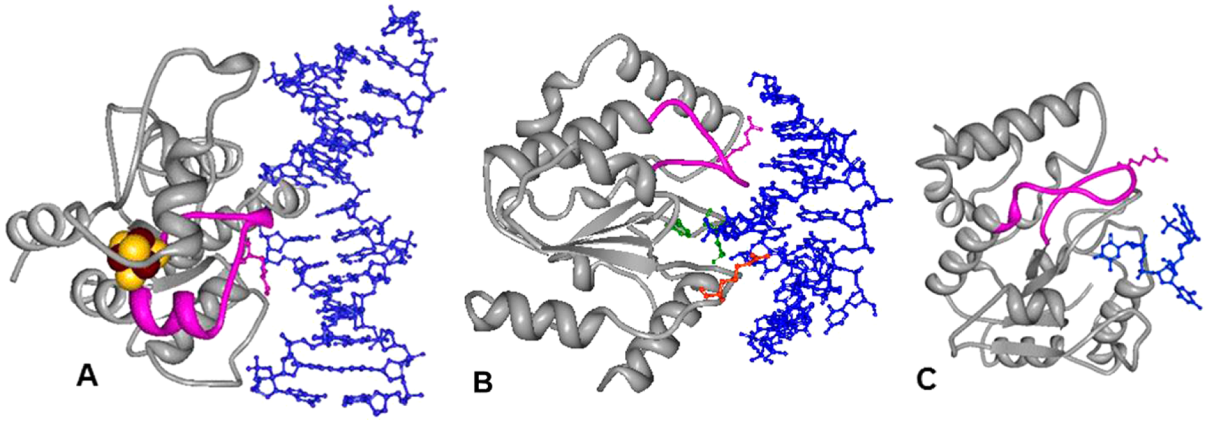

Figure 8. A view of the pseudo-FCL motif in TTB bound to AP site-containing DNA (A) and the analogous loop in other members of the UDG superfamily, human UDG bound uracil-AP site DNA (B) and Herpes simplex virus UDG bound to a uracil-containing trinucleotide (C). Figures were prepared from coordinates deposited in the Protein Database, accession codes 2DDG, 1SSP, and 1LAU, respectively. The DNA is shown in blue. Residues that make up the pseudo-FCL and analogous motifs are highlighted in fuchsia with a conserved Arg residue within this loop motif in each enzyme represented in a ball-and-stick model. Human UDG Arg 276, which has previously been shown to be important for binding and uracil removal, is colored in orange in ball and stick representation. The uracil and phosphate of the DNA is shown in ball and stick and green.

Moreover, replacement of Arg 86 with alanine reveals that Arg 86 makes specific contacts that are critical for binding and removal of uracil in double-stranded DNA. The fluorescence anisotropy assays indicated that R86A AFUDG has a severely compromised ability to bind double-stranded DNA containing the product analogue. In addition, in single-turnover uracil excision assays, R86A exhibited a 2.5-fold slower rate of uracil removal (k_2) from the double-stranded DNA substrate compared to WT AFUDG. Notably, the ability of R86A AFUDG to cleave uracil from single-stranded DNA was unaffected, with rates similar to WT. Enzyme-mediated uracil cleavage requires access to the glycosidic bond to allow for placement within a base specific pocket and proximity to catalytic residues. The lack of base pairing in single-stranded DNA may provide AFUDG with easier access to uracil and may therefore have less dependence on interactions mediated by Arg 86. In contrast, in double-stranded DNA more extensive contacts are likely required to induce bending and prying open of the DNA duplex in order to promote uracil expulsion. Indeed, an overlay of crystal structures from a family 4 UDG (TTA) with a cocrystal structure of TTB with abasic site-containing duplex DNA (Figure 2) suggests that the Arg 86 side-chain is close enough (3.4 Å) to hydrogen bond with the backbone of the uracil-containing strand. In analogous studies with *E. coli* MutY, replacement of Lys 198 with alanine resulted in a decreased rate for removal (15-fold) of adenine opposite G under STO conditions.[21] In addition, K198A MutY exhibited decreased affinity (10−20-fold) for duplex DNA containing OG or G paired with the noncleavable substrate analogue, 2′-deoxy-2′-fluoroadenosine (FA). Despite the reduced affinity with the OG:FA duplex, K198A exhibited similar processing of an OG:A substrate as WT MutY, illustrating that the catalytic defect was only readily observed using the nonoptimal substrate under STO conditions. In both MutY and AFUDG, replacements of positively charged residues in the loop region result in altered efficiency of base removal or damage affinity, suggesting similar roles of the two motifs in damage detection and repair.

In the structure of human UDG,[38] there are 5 arginine and 8 lysine residues localized to the active site face of the enzyme. Of these, an Arg residue (Arg 276) located in the highly conserved "leucine loop" motif was observed to be in close contact with the DNA phosphate backbone adjacent to a uracil nucleotide in the X-ray structure (Figure 8B). In addition, mutation of Arg 276 to a variety of different amino acids was extensively examined.[39,40] Interestingly, mutation of Arg 276 to alanine showed a 4-fold reduction in k_{cat} for the excision of uracil in a ds DNA context but caused no change in processing of uracil within ss DNA. This result is remarkably similar to what we observed herein with R86A AFUDG, despite the more distant location of Arg 86 from the site of uracil excision. Further inspection of the reported structures of family 1 UDGs indicates the presence of a region corresponding to the pseudo-FCL motif in AFUDG but distinct from the motif harboring Arg 276 in human UDG (Figure 8, Figure S3). In the family 1 UDGs, this loop is anchored on each end with an α helix as opposed to the $[4Fe{-}4S]^{2+}$ cluster found in the family 4 and 5 UDGs.

It is intriguing to consider that there are advantages to having an iron−sulfur cluster to anchor the motif in the thermophilic UDG enzymes over α-helices found in the family 1 UDGs. The $[4Fe{-}4S]^{2+}$ may provide additional stability to the large and flexible pseudo-FCL motif. The importance of the anchoring function is reflected by decreased rates (k_2) of uracil cleavage for both C85A and C101A AFUDG. Mutation of the Cys ligands involved in tethering the loop motif through coordination to the iron−sulfur cluster to a noncoordinating residue like alanine would be expected to alter the stability and structure of the pseudo-FCL region, which in turn may reduce the ability of the pseudo-FCL motif to properly engage the DNA substrate to mediate uracil excision. Though stability is important, a previous report using tryptophan fluorescence has also shown an importance of dynamics and flexibility.[36] This study showed that at low temperatures AFUDG adopts a compact, closed conformation and has low enzyme activity; however, at higher temperatures where AFUDG is more active, a more open and dynamic conformation was observed.[36] Metal ion coordination of the peptide loop in AFUDG may provide the required balance between stability and flexibility. Indeed, the ability to provide for both flexibility and stability may be an underappreciated benefit of the use of metal coordination in proteins over hydrogen bonding to stabilize loops and interactions between protein domains. Analogous properties

dx.doi.org/10.1021/bi3000462 | *Biochemistry* 2012, 51, 5187−5197

have been observed in the field of supramolecular chemistry where the use of metal coordination instead of hydrogen-bonding interactions provides for desirable properties including reversibility in complex assembly, robustness to a variety of solvents, and unique architectures.[41]

There are now many examples of iron−sulfur clusters in nucleic acid processing enzymes involved in a wide array of key processes including DNA repair and replication, transcription, and RNA modification.[42] Many of these enzymes, like AFUDG, catalyze reactions that do not require electron transfer or utilize cluster-mediated catalysis; however, we suggest that iron−sulfur clusters play much more than a spectrator role in nucleic acid processing. Indeed, like the clusters in HhH glycosylases and family 4 UDGs, iron−sulfur clusters in nucleic acid processing enzymes may play important roles in mediating interactions with the nucleic acid substrate and protein partners. In fact, in several reports, disruption of iron−sulfur cluster coordination has been shown to alter nucleic acid or protein partner binding.[42,43] In addition, the redox status of the cell may serve to modulate the oxidation state or presence of the iron−sulfur cluster in these enzymes to further alter protein−nucleic acid interactions, providing a mechanism for fine-tuning the complex cellular processes mediated by nucleic acid processing enzymes.

■ ASSOCIATED CONTENT

Supporting Information

EPR spectroscopy of C85A, C101A, and WT AFUDG, stability assays of C85A, C101A, K100A, and WT AFUDG, sequence alignment of family 1 versus family 4/5 UDGs. This material is available free of charge via the Internet at http://pubs.acs.org.

■ AUTHOR INFORMATION

Corresponding Author

*E-mail ssdavid@ucdavis.edu; tel 530-752-4280; fax 530-752-8147.

Funding

This work was supported by a grant from the National Cancer Institute of the National Institutes of Health to S.S.D. (CA67985) and SEED funding from the University of Utah.

Notes

The authors declare no competing financial interest.

■ ACKNOWLEDGMENTS

We acknowledge the generous and helpful start given to us by Dr. William A. Franklin (d. 2009). In addition to providing the AFUDG gene-containing plasmid, we appreciate his enthusiastic encouragement to pursue work on this enzyme and useful advice. Dr. Hans-Joachim Fritz (Georg-August-Universitat, Gottingen) provided the plasmid for TTB UDG. EPR spectroscopy was carried out with the help of Dr. R. David Britt and Jamie Stull (University of California, Davis) and Dr. Lance Seefeldt (Utah State). We also thank Dr. Clark Lagarias for use of a fluorescence anisotropy instrument as well as Dr. Nathan Rockwell for help with instrument setup and use (University of California, Davis). In addition, we gratefully acknowledge the experimental assistance of Tram Anh Dao and Tai Holland in performing the site-directed mutagenesis to prepare R86A, R91A, and K100A mutations in AFUDG. We also thank Dr. Momchilo Vuyisich for initial work on AFUDG expression and purification and site-directed mutagenesis to make C85A and C101A mutations.

■ DEDICATION

This paper is dedicated to the discoverer of AFUDG, Dr. William A. Franklin (d. 9/19/2009).

■ ABBREVIATIONS

AFUDG, *Archeoglobus fulgidus* uracil DNA glycosylase; AP, apurinic-apyrimidinic; BER, base excision repair; bp, base pair; ds, double-stranded; ECUDG, *Escherichia coli* uracil DNA glycosylase; EDTA, ethylenediaminetetraacetic acid; Endo III, endonuclease III; FCL, iron−sulfur cluster loop; HhH, helix−hairpin−helix; hUDG, human uracil DNA glycosylase; IPTG, isoproylplthiogalactoside; MTO, multiple-turnover; OG, 8-oxo-7,8-dihydroguanine; PAGE, polyacrylamide gel electrophoresis; PMSF, phenylmethylsulfonyl fluoride; PNK, polynucleotide kinase; RhX, X-Rhodamine, 5,6-isothiocyanate; ss, single-stranded; STO, single-turnover; THF, tetrahydrofuran nucleotide (abasic site analogue); TMUDG, *Thermatoga maritima* uracil DNA glycosylase; TTA, *Thermus thermophilus* uracil DNA glycosylase A; TTB, *Thermus thermophilus* uracil DNA glycosylase B; UDG, uracil DNA glycosylase.

■ REFERENCES

(1) David, S. S., and Williams, S. D. (1998) Chemistry of Glycosylases and Endonucleases Involved in Base-Excision Repair. *Chem. Rev. 98*, 1221−1262.

(2) Lindahl, T. (1993) Instability and decay of the primary structure of DNA. *Nature 362*, 709−715.

(3) Tye, B. K., Nyman, P. O., Lehman, I. R., Hochhauser, S., and Weiss, B. (1977) Transient accumulation of Okazaki fragments as a result of uracil incorporation into nascent DNA. *Proc. Natl. Acad. Sci. U. S. A. 74*, 154−157.

(4) Pearl, L. H. (2000) Structure and function in the uracil-DNA glycosylase superfamily. *Mutat. Res. 460*, 165−181.

(5) Lee, H. W., Dominy, B. N., and Cao, W. (2012) A new family of deamination repair enzymes in the uracil DNA glycosylase superfamily. *J. Biol. Chem.,*.

(6) Savva, R., McAuley-Hecht, K., Brown, T., and Pearl, L. (1995) The structural basis of specific base-excision repair by uracil-DNA glycosylase. *Nature 373*, 487−493.

(7) Mol, C. D., Arvai, A. S., Slupphaug, G., Kavli, B., Alseth, I., Krokan, H. E., and Tainer, J. A. (1995) Crystal structure and mutational analysis of human uracil-DNA glycosylase: structural basis for specificity and catalysis. *Cell 80*, 869−878.

(8) Slupphaug, G., Mol, C. D., Kavli, B., Arvai, A. S., Krokan, H. E., and Tainer, J. A. (1996) A nucleotide-flipping mechanism from the structure of human uracil-DNA glycosylase bound to DNA. *Nature 384*, 87−92.

(9) Werner, R. M., and Stivers, J. T. (2000) Kinetic isotope effect studies of the reaction catalyzed by uracil DNA glycosylase: evidence for an oxocarbenium ion-uracil anion intermediate. *Biochemistry 39*, 14054−14064.

(10) Stivers, J. T., Pankiewicz, K. W., and Watanabe, K. A. (1999) Kinetic mechanism of damage site recognition and uracil flipping by Escherichia coli uracil DNA glycosylase. *Biochemistry 38*, 952−963.

(11) Lindahl, T., and Nyberg, B. (1974) Heat-induced deamination of cytosine residues in deoxyribonucleic acid. *Biochemistry 13*, 3405−3410.

(12) Sandigursky, M., and Franklin, W. A. (1999) Thermostable uracil-DNA glycosylase from Thermotoga maritima a member of a novel class of DNA repair enzymes. *Curr. Biol. 9*, 531−534.

(13) Starkuviene, V., and Fritz, H. J. (2002) A novel type of uracil-DNA glycosylase mediating repair of hydrolytic DNA damage in the extremely thermophilic eubacterium Thermus thermophilus. *Nucleic Acids Res. 30*, 2097−2102.

(14) Sandigursky, M., and Franklin, W. A. (2000) Uracil-DNA glycosylase in the extreme thermophile Archaeoglobus fulgidus. *J. Biol. Chem. 275*, 19146−19149.
(15) Boal, A. K., Yavin, E., Lukianova, O. A., O'Shea, V. L., David, S. S., and Barton, J. K. (2005) DNA-bound redox activity of DNA repair glycosylases containing [4Fe-4S] clusters. *Biochemistry 44*, 8397−8407.
(16) Hinks, J. A., Evans, M. C., De Miguel, Y., Sartori, A. A., Jiricny, J., and Pearl, L. H. (2002) An iron-sulfur cluster in the family 4 uracil-DNA glycosylases. *J. Biol. Chem. 277*, 16936−16940.
(17) Kosaka, H., Hoseki, J., Nakagawa, N., Kuramitsu, S., and Masui, R. (2007) Crystal structure of family 5 uracil-DNA glycosylase bound to DNA. *J. Mol. Biol. 373*, 839−850.
(18) Hoseki, J., Okamoto, A., Masui, R., Shibata, T., Inoue, Y., Yokoyama, S., and Kuramitsu, S. (2003) Crystal structure of a family 4 uracil-DNA glycosylase from Thermus thermophilus HB8. *J. Mol. Biol. 333*, 515−526.
(19) Porello, S. L., Cannon, M. J., and David, S. S. (1998) A substrate recognition role for the [4Fe-4S]2+ cluster of the DNA repair glycosylase MutY. *Biochemistry 37*, 6465−6475.
(20) Cunningham, R. P., Asahara, H., Bank, J. F., Scholes, C. P., Salerno, J. C., Surerus, K., Munck, E., McCracken, J., Peisach, J., and Emptage, M. H. (1989) Endonuclease III is an iron-sulfur protein. *Biochemistry 28*, 4450−4455.
(21) Chepanoske, C. L., Golinelli, M. P., Williams, S. D., and David, S. S. (2000) Positively charged residues within the iron-sulfur cluster loop of E. coli MutY participate in damage recognition and removal. *Arch. Biochem. Biophys. 380*, 11−19.
(22) Thayer, M. M., Ahern, H., Xing, D., Cunningham, R. P., and Tainer, J. A. (1995) Novel DNA binding motifs in the DNA repair enzyme endonuclease III crystal structure. *EMBO J. 14*, 4108−4120.
(23) Lukianova, O. A., and David, S. S. (2005) A role for iron-sulfur clusters in DNA repair. *Curr. Opin. Chem. Biol. 9*, 145−151.
(24) Sambrook, J., and Maniatis, T. (1989) *Molecular Cloning: A Laboratory Manual*, 2nd ed., Cold Spring Harbor Press, Cold Spring Harbor, NY.
(25) Shaw, R. W., Feller, J. A., and Bloom, L. B. (2004) Contribution of a conserved phenylalanine residue to the activity of Escherichia coli uracil DNA glycosylase. *DNA Repair 3*, 1273−1283.
(26) Maher, R. L., and Bloom, L. B. (2007) Pre-steady-state kinetic characterization of the AP endonuclease activity of human AP endonuclease 1. *J. Biol. Chem. 282*, 30577−30585.
(27) Fersht, A. (1985) *Enzyme Structure and Mechanism*, W.H. Freeman and Co., New York.
(28) Porello, S. L., Leyes, A. E., and David, S. S. (1998) Single-turnover and pre-steady-state kinetics of the reaction of the adenine glycosylase MutY with mismatch-containing DNA substrates. *Biochemistry 37*, 14756−14764.
(29) Fersht, A. (1999) *Structure and Mechanism in Protein Science: A Guide to Enzyme Catalysis and Protein Folding*, W.H. Freeman and Co., New York.
(30) Golinelli, M. P., Chmiel, N. H., and David, S. S. (1999) Site-directed mutagenesis of the cysteine ligands to the [4Fe-4S] cluster of Escherichia coli MutY. *Biochemistry 38*, 6997−7007.
(31) Lindahl, T. (1974) An N-glycosidase from Escherichia coli that releases free uracil from DNA containing deaminated cytosine residues. *Proc. Natl. Acad. Sci. U. S. A. 71*, 3649−3653.
(32) Parikh, S. S., Putnam, C. D., and Tainer, J. A. (2000) Lessons learned from structural results on uracil-DNA glycosylase. *Mutat. Res. 460*, 183−199.
(33) Zharkov, D. O., Mechetin, G. V., and Nevinsky, G. A. (2010) Uracil-DNA glycosylase: Structural, thermodynamic and kinetic aspects of lesion search and recognition. *Mutat. Res. 685*, 11−20.
(34) Slupphaug, G., Olsen, L. C., Helland, D., Aasland, R., and Krokan, H. E. (1991) Cell cycle regulation and in vitro hybrid arrest analysis of the major human uracil-DNA glycosylase. *Nucleic Acids Res. 19*, 5131−5137.
(35) Krokan, H. E., Drablos, F., and Slupphaug, G. (2002) Uracil in DNA--occurrence, consequences and repair. *Oncogene 21*, 8935−8948.
(36) Knaevelsrud, I., Ruoff, P., Anensen, H., Klungland, A., Bjelland, S., and Birkeland, N. K. (2001) Excision of uracil from DNA by the hyperthermophilic Afung protein is dependent on the opposite base and stimulated by heat-induced transition to a more open structure. *Mutat. Res. 487*, 173−190.
(37) Rothschild, L. J., and Mancinelli, R. L. (2001) Life in extreme environments. *Nature 409*, 1092−1102.
(38) Parikh, S. S., Mol, C. D., Slupphaug, G., Bharati, S., Krokan, H. E., and Tainer, J. A. (1998) Base excision repair initiation revealed by crystal structures and binding kinetics of human uracil-DNA glycosylase with DNA. *EMBO J. 17*, 5214−5226.
(39) Chen, C.-Y., Mosbaugh, D. W., and Bennet, S. E. (2004) Mutational Analysis of Arginine 276 in the Leucine-loop of Human Uracil-DNA Glycosylase. *J. Biol. Chem. 279*, 48177−48188.
(40) Chen, C.-Y., Mosbaugh, D. W., and Bennet, S. E. (2005) Mutations at Arginine 276 transform human uracil-DNA glycosylase into a single-stranded DNA-specific uracil-DNA glycosylase. *DNA Repair 4*, 793−805.
(41) Hof, F., Craig, S. L., Nuckolls, C., and Rebek, J. (2002) Molecular Encapsulation. *Angew. Chem., Int. Ed. 41*, 1488−1508.
(42) White, M. F., and Dillingham, M. S. (2011) Iron-sulphur clusters in nucleic acid processing enzymes. *Curr. Opin. Struct. Biol 22*, 1−7.
(43) Netz, D. J. A., Stith, C. M., Stumpfig, M., Kopf, G., Vogel, D., Genau, H. M., Stodola, J. L., Lill, R., Burgers, P. M. J., and Pierik, A. J. (2011) Eukaryotic DNA polymerases require an iron-sulfur cluster for the formation of active complexes. *Nat. Chem. Biol. 8*, 125−132.